



Cite this: *Chem. Sci.*, 2025, **16**, 20422

All publication charges for this article have been paid for by the Royal Society of Chemistry

N-heterocyclic carbenes as clickable molecular anchors for electrochemical surface functionalization of metals and glassy carbon

Antoine Juneau,^{id,ab} Ahmadreza Nezamzadeh,^{id,bc} Béatrice Laberge,^{id,ab} Anastasia Messina,^{id,bc} Justin Lomax,^{id,bd} Thilini M. Suduwella,^{id,ab} Jashanpreet Kaur,^{id,ab} Vikram Singh,^{id,ab} Mark D. Aloisio,^{id,bc} Paul J. Ragogna,^{id,*bd} Cathleen M. Crudden,^{id,*bc} and Janine Mauzeroll,^{id,*ab}

The potential of alkyne-containing NHCs as anchor molecules for electrochemical surface modification is investigated. Using a combination of X-ray photoelectron spectroscopy, atomic force microscopy, fluorescence tagging, and shell-isolated nanoparticle-enhanced Raman spectroscopy, we demonstrate that these NHCs can bind effectively to multiple surfaces and be functionalized via electrochemical copper-catalyzed azide–alkyne cycloaddition. Notably, we extend the scope of substrates beyond metals by demonstrating successful modification of glassy carbon. Compared to diazonium salts, NHC coatings show comparable resistance to sonication while forming films of only \sim 4 nm in thickness. This reduced film thickness leads to lower surface passivation, which could offer advantages for electrochemical applications. The versatility of these NHC as molecular anchors is demonstrated through the attachment of electrochemically active TEMPO⁺, the immobilization of streptavidin, and the formation of copper coatings. These findings highlight the potential of NHCs as alternatives to thiols and diazonium salts for the design of functional materials, electrodes, and biosensors.

Received 28th May 2025
Accepted 23rd September 2025

DOI: 10.1039/d5sc03908h
rsc.li/chemical-science

Introduction

Since first being described more than 60 years ago,^{1,2} N-heterocyclic carbenes (NHCs) have become ubiquitous in organocatalysis, organometallic synthesis, and homogeneous transition metal catalysis.^{3–5} However, over the past decade, their ability to form strong covalent bonds with metals in various forms has also driven significant interest in the field of materials science.^{6–9}

NHCs form self-assembled monolayers (SAMs) or films on a wide range of metal surfaces. While considerable focus has been on gold surfaces,^{10–16} they have also been shown to bind to numerous metals, including copper,^{12,14,17–19} platinum,^{20–22} palladium,^{20,23} titanium,²⁴ iron,²⁴ cobalt,²⁵ silver,^{12,26} magnesium,²⁷ ruthenium,^{22,25} and alloys like steel.²⁸ On oxides, NHCs were found to bind with surface lattice oxygen.²⁴ On metallic gold and copper surfaces, they rather bond directly with adatoms in either a flat-lying or upright configuration, largely

depending on the steric properties of their N-substituents.¹⁴ This interaction with adatoms is likely the origin of NHC's mobility on planar surfaces, allowing them to self-assemble.¹⁶

The ability of NHCs to form dynamic yet robust bonds with metal surfaces has made them promising tools for surface modification. They are now being used for a growing number of applications, including corrosion mitigation,^{27,29–31} nanoparticle decoration^{32–35} (including atomically precise nanoparticles^{36,37}), and functional surface coatings.^{9,38,39} Notably, the incorporation of azido or alkyne functional groups into NHCs has expanded their role as molecular anchors, allowing surface functionalization with a wide range of molecules *via* click chemistry. For instance, alkyne-NHC and azido-NHC have been used to attach ferrocene,⁴⁰ mannose,⁴¹ and biotin^{41,42} on gold surfaces (e.g. Gupta group, Fig. 1a). Importantly, a similar demonstration was achieved on graphene,⁴³ demonstrating the ability of the NHC to form a covalent bond with carbon (Kwon group, Fig. 1a). Compared to thiol monolayers, NHC SAMs have been found to have higher binding energies on gold,¹¹ are thermally stable up to \geq 573 K,^{11,44} resist sonication,⁴⁵ withstand large pH ranges (2–12),⁴⁰ and, contrary to thiols, survive chemical oxidants such as H₂O₂.⁴⁰ Despite the potential of NHCs as molecular anchors, current studies mostly focus on gold surfaces, and the ability to functionalize NHCs after deposition remains limited.

Herein, we demonstrate that NHCs serve as molecular anchors and participate in electro-promoted click reactions,

^aDepartment of Chemistry, McGill University, Montréal, Québec, H3A 0B8, Canada.
E-mail: janine.mauzeroll@mcgill.ca

^bCarbon to Metal Coating Institute, Queen's University, Kingston, Ontario K7L 3N6, Canada

^cDepartment of Chemistry, Queen's University, Kingston, Ontario K7L 3N6, Canada

^dDepartment of Chemistry, University of Western Ontario, London, Ontario, N6A 3K7, Canada



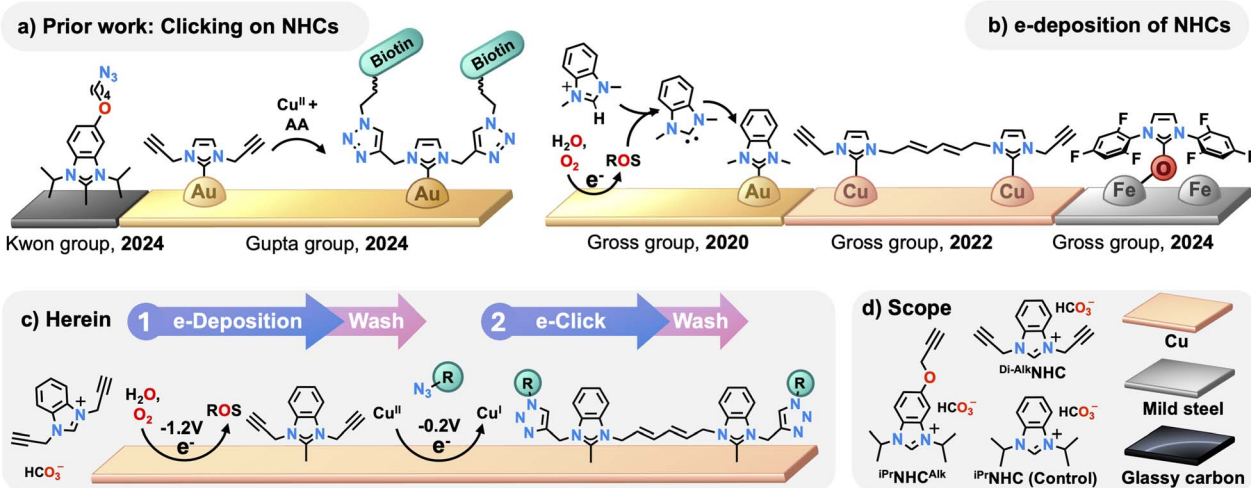


Fig. 1 (a) Previous studies demonstrating the clicking of alkyne-functionalized NHCs using ascorbic acid (AA) as chemical reducing agent.^{42,43} (b) Prior work on the electrodeposition of NHCs onto various metals and metal oxides *via* generation of reactive oxygen species like HO⁻.^{24,29,46} (c) This study: electrodeposition of NHCs using imidazolium bicarbonate salts as carbene precursors in a solution composed of supporting electrolyte in CH₃CN with 0.1% v/v H₂O as the source of reactive oxygen species. The deposition is achieved using 25 pulses of 5 s at -1.2 V, each followed by a 5 s relaxation. The electro-click reaction is conducted in a solution of CuSO₄ (0.1 mM) with supporting electrolyte (50 mM) in CH₃CN, applying a constant potential of -0.2 V for 15 min. (d) Scope of the substrates and NHCs precursors used herein.

enabling facile functionalization of various surfaces (Fig. 1c and d). This approach is validated using two imidazolium bicarbonate salt precursors bearing alkyne moieties, namely ^{iPr}NHC^{Alk} and ^{Di-Alk}NHC (Fig. 1d). The former features an alkyne group expected to orient perpendicular to the surface. In contrast, the latter contains two alkyne groups aligned parallel to the surface, allowing for lateral cross-linking between molecules.²⁹ As negative control, a non-alkyne NHC was also employed (^{iPr}NHC). To explore substrate versatility, we selected three conductive materials. Copper was chosen for its well-established interaction with NHCs.⁴⁶ Low carbon steel (also known as *mild steel*), valued for its malleability and ductility, was included because of its broad industrial applications.⁴⁷ Glassy carbon (GC) was selected due to its widespread use as electrode material. Notably, this study represents the first demonstration of NHC anchoring on glassy carbon, offering a lightweight, inert alternative to metal-based electrodes, and offering a versatile platform for the functionalization of carbon-based materials. Using X-ray photoelectron spectroscopy (XPS), shell-isolated nanoparticle-enhanced Raman spectroscopy (SHINERS), fluorescence tagging and atomic force microscopy (AFM), we demonstrate the efficient post-deposition functionalization of these surfaces.

This work builds on previously reported electrodeposition methods, which have emerged as powerful tools for coating conductive materials with NHCs (Fig. 1b).^{24,29,46,48} This process is said to involve the cathodic formation of reactive oxygen species (ROS) and HO⁻, which can deprotonate the imidazolium precursor to form its corresponding carbene; the intermediate central to NHC's reactivity with surfaces.⁴⁶

Surface analysis by X-ray photoelectron spectroscopy (XPS)

We started our investigation by using XPS to monitor the changes in the N 1s signal at each step of the functionalization

process. Fig. 2a shows the results obtained when using polished steel modified with ^{iPr}NHC^{Alk}. A residual nitrogen signal (400.4 eV), attributed to surface or sub-surface impurities, could not be avoided and is seen in the unfunctionalized sample (Fig. 2a). The deposition of ^{iPr}NHC^{Alk} was achieved electrochemically by applying 25 cycles of 5 seconds pulses at a potential of -1.2 V. The sample was then rinsed with CH₃CN and EtOH to remove adsorbed precursor, electrolyte, and byproducts. After this procedure, we observed an increase in the N 1s signal, which could be fitted into three components (Fig. 2b). The peaks at 401.8 and 400.2 eV agree perfectly with the literature for similar NHC structures on iron oxide.²⁴ We attribute the former to quaternary ammonium (N⁺ species) impurities and the second at 400.2 eV to surface-bound NHC.²⁴ The shift towards lower binding energies, from the precursor (401.1 eV)³¹ to surface-bound NHC (400.2 eV), agrees with other reports^{24,29} and with DFT prediction (represented as red dots on Fig. 2a). A third peak at 398.9 eV was also observed and is attributed to neutral byproducts, similar to other reports for X-ray induced NHC byproducts.²⁸

Functionalization of the surface was next carried out by performing an electro-click reaction with 1-azido-hexane in the presence of 0.1 mM Cu^{II}. A constant potential of -0.2 V was applied for 15 minutes to enable reduction into catalytically active Cu^I.⁴⁹ The resulting N 1s signal was too complex for unambiguous deconvolution; nevertheless, increased signal intensity is observed in the area where triazole signals are expected.⁵⁰ As shown in Fig. 2c, the nitrogen atomic percentage (N%) detected on the surface roughly tripled after the click reaction (from 0.9% to 2.9%), close to the $\times 2.5$ increase expected from the click reaction. For copper and GC, the signal was too complex to be fitted, but an increase in N% was also observed (see SI, Fig. S16).



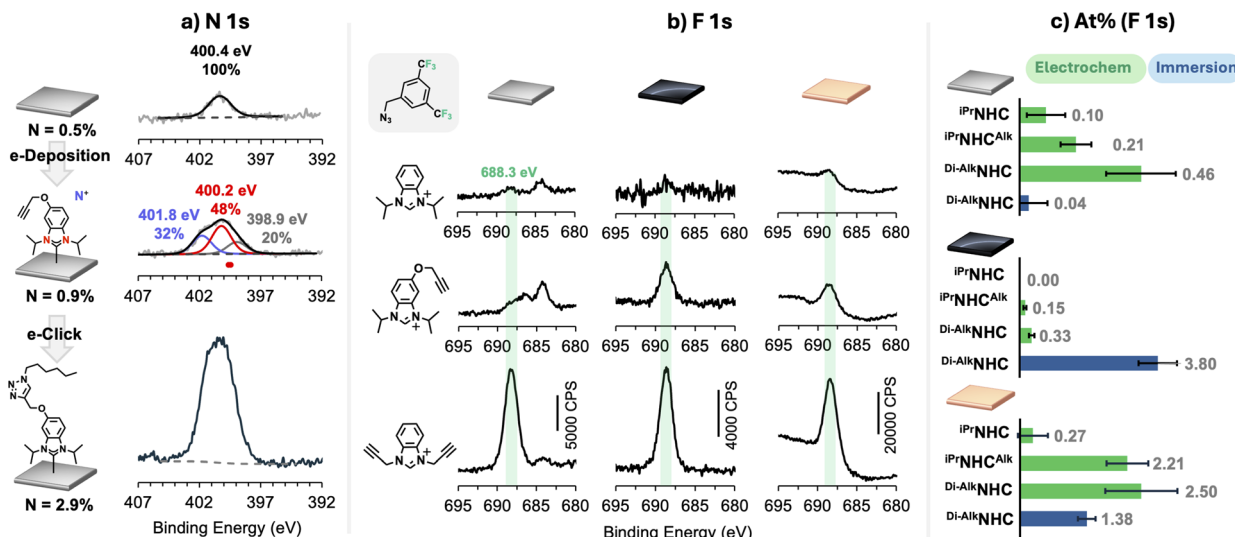


Fig. 2 (a) XPS measurements showing the progressive increase of the N 1s signal at each step of the functionalization process for steel functionalized with $^{iPr}\text{NHC}^{\text{Alk}}$ and 1-azidohexane. (b) F 1s spectra recorded for surfaces functionalized with three different NHCs and a CF_3 -tagged azide. The signal at 688.3 eV is attributed to CF_3 , while the signal at 684 eV on steel corresponds to residual electrolyte (NBu_4PF_6). For GC and Cu substrates, the electrolytes KPF_6 and NaI were used, respectively. Note that for GC, the azide was clicked via NaAsc reduction of Cu^{II} , while for steel and Cu, it was done from electrochemical reduction of Cu^{II} . (c) Comparison of the atomic % F 1s content in each sample from survey XPS measurements. Error bars represent four measurements taken at different spots on the same sample. Note that the scale differs between substrates. The electrochemical method (green bar) is compared with the immersion method (blue bar) for $^{\text{Di-Alk}}\text{NHC}$ in MeOH .

Successful functionalization of the surface-bound NHCs was further confirmed by attachment of a fluorine-labeled azide (N_3 -benzyl-(CF_3)₂). Fig. 2b shows the recorded F 1s spectra, obtained after rinsing with H_2O , EtOH and CH_3CN , and sonicating the samples in a 1 : 1 mixture of CH_3CN and H_2O for 10 minutes. As expected, the control experiments functionalized with ^{iPr}NHC showed weak or no F 1s signal, while samples functionalized with ^{Alk}NHC and $^{Di-Alk}NHC$ showed organic fluoride signal at 688 eV. This confirms that the presence of alkyne groups is necessary for azide attachment. Interestingly, $^{Di-Alk}NHC$ resulted in a greater F 1s signal for all substrates, as quantified from XPS survey experiments (Fig. 2c). We attribute this performance to $^{Di-Alk}NHC$'s ability to form a multilayer *via* alkyne polymerization (*vide infra*).

Another noteworthy result is that the method succeeded on glassy carbon. While NHC's interaction with metal is now well known, its interaction with GC is more surprising given that carbenes cannot form dative bonds with carbon atoms. There is only one report of NHC functionalization on carbon-based materials, namely graphene,⁴³ in which the authors suggest that NHC binds by attack on the graphene C=C bond, forming a cyclopropane adduct. In our case, NHCs may bind through a similar mechanism, but could also interact with the oxides or surface defects that are introduced during the electrochemical activation process (see Experimental section for more details).

We next tested whether the electrochemical method offered an advantage over other deposition methods. NHCs are often deposited by immersing the substrate in an NHC solution for an extended period (referred here as immersion method). This technique, reported by us and others, has proven effective for various metals including copper⁵¹ and steel.²⁸ Two samples were

prepared by immersion in a 5 mM solution of $^{Di-Alk}NHC$ in MeOH for 66 hours, followed by chemical clicking of the fluorinated azide *via* NaAsc reduction of Cu^{II} . The atomic % obtained from XPS survey spectra revealed that, for metallic substrates, the immersion method was less effective than the electrochemical method, resulting in 1.8-fold and 10-fold lower surface coverage on Cu and steel, respectively. In contrast, for GC, immersion deposition produced a more than 10-fold higher surface coverage.

Finally, a one-pot approach, where deposition and the click reaction occurred simultaneously, was also tested (see SI, section 6). However, it yielded lower surface coverage, making the two-step process the more effective strategy.

To bring further evidence for the successful azide-alkyne cycloaddition, we resorted to Raman spectroscopy.

Shell-isolated nanoparticles enhanced Raman spectroscopy (SHINERS)

Surface-enhanced Raman spectroscopy (SERS) has been employed to detect NHCs on copper substrates⁴⁸ and gold nanoparticles,⁵² because the plasmonic properties of these metals amplify the otherwise weak signal from surface-bound species. In the case of steel or glassy carbon, however, direct Raman spectroscopy is not feasible due to iron's lack of plasmonic character. For example, the Raman spectra of steel functionalized with ^{Di-Alk}NHC yielded only noise-level signals, with no detectable vibrational bands that could be ascribed to its two alkyne substituents (Fig. 3a, blue trace). A strong signal could, however, be observed after depositing plasmonic nanoparticles onto the surface using the method known as

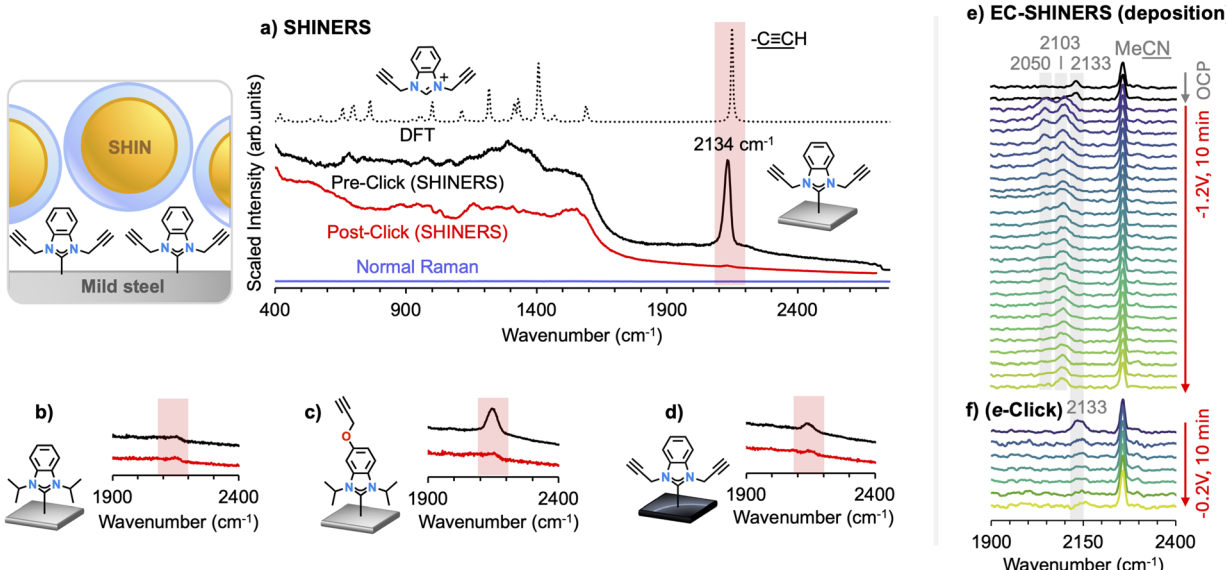


Fig. 3 (a) SHINERS of steel surfaces functionalized with $^{Di\text{-Alk}}\text{NHC}$ before and after electro-clicking with an azido-functionalized polyethylene glycol unit ($\text{N}_3\text{-PEG}_{23}\text{-N}_3$). Due to inhomogeneous nature in SHINs amplification, intensities were scaled to normalize the baseline and are therefore purely qualitative. The DFT-predicted Raman spectrum (dashed line) was calculated at the B3LYP/6-311+G(2d,2p) level of theory with SMD: CH_3CN solvation. The normal Raman spectra, obtained before addition of SHINs, showed no discernible signal (blue trace) (b–d). Similar experiments were performed on various NHC-substrate combinations, highlighting changes in the triple bond peak after clicking. In these cases, clicking was carried out chemically *via* CuSO_4 reduction with NaAsc . (e) *In situ* EC-SHINERS experiments tracking the evolution of the triple bond region during electrochemical reduction of $10\text{ mM }^{Di\text{-Alk}}\text{NHC}$ in CH_3CN with $0.1\% \text{ v/v H}_2\text{O}$ and 50 mM NaI . (e) Similar methodology applied for electro-clicking, using a $^{Di\text{-Alk}}\text{NHC}$ -coated steel surface as working electrode, submerged in CuSO_4 (0.1 mM), $\text{N}_3\text{-PEG}_4\text{-biotin}$ (1.75 mM) and NBu_4PF_6 (50 mM) in CH_3CN . Spectra were recorded at intervals of 25 s for (e) and 100 s for (f). OCP stands for open circuit potential.

SHINERS.^{53,54} In brief, this approach consists of covering the surface with a thin layer of shell-isolated nanoparticles (SHINs), which are composed of a gold core encased in a silica shell. These nanoparticles amplify the electric field at their proximity, creating so called “hotspots” that enhance inelastic scattering. The shell acts as a protective barrier, preventing possible chemical reaction between the NHCs and the gold surface.

SHINERS spectra obtained in this manner for a series of NHC on steel and glassy carbon are shown in Fig. 3a–d. The strongest signal was obtained for $^{Di\text{-Alk}}\text{NHC}$ deposited on steel (Fig. 3a), making it the primary focus of our analysis. Prior to the click reaction, the NHC-functionalized steel surface showed a prominent peak at 2134 cm^{-1} , characteristic of $\text{C}\equiv\text{C}$ stretching, attributed to surface-bound $^{Di\text{-Alk}}\text{NHC}$. The DFT-predicted spectrum of the imidazolium precursor of $^{Di\text{-Alk}}\text{NHC}$ (Fig. 3a, black dotted line) provides an estimate of the expected band positions for NHC related compound and is in good agreement with the observed $\text{C}\equiv\text{C}$ frequency. Additional peaks were observed in the fingerprint region ($300\text{--}1900\text{ cm}^{-1}$); however, the intrinsic signals from the nanoparticles (Fig. S12, SI) and the broad nature of these bands makes a precise assignment in this region challenging. Nonetheless, presence of signal in the fingerprint region along with the strong alkyne signal at 2134 cm^{-1} is consistent with the formation of an organic layer containing $\text{C}\equiv\text{C}$ triple bonds, supporting the presence of $^{Di\text{-Alk}}\text{NHC}$ on steel.

A previous study using similar electrochemical methods to deposit alkyne-NHCs on copper have provided evidence of

polymerization *via* the triple bond, resulting in a layer of $\sim 2\text{ nm}$ thickness (Fig. 1a, Gross group 2022).²⁹ This process was shown to occur *via* deprotonation of the alkyne, leading to the formation of acetylide ions ($\text{C}\equiv\text{C}^-$), which then initiate polymerization. Notably, the authors could suppress the polymerization process by protonating the acetylide using ascorbic acid, leading to the formation of a single monolayer. Our results demonstrate that despite the polymerization process, triple bonds remain in sufficiently high concentrations to be detected. This retention of the $\text{C}\equiv\text{C}$ moiety confirms the material is suitable for further functionalization through CuAAC. Indeed, after coupling the NHC topcoat to an azido-PEG chain ($\text{N}_3\text{-PEG}_{24}\text{-N}_3$) *via* e-click, the $\text{C}\equiv\text{C}$ stretch became undetectable, indicating complete click reaction (Fig. 3a, red trace).

Similar observations were made for $^{i\text{Pr}}\text{NHC}^{\text{Alk}}$ -functionalized steel and $^{Di\text{-Alk}}\text{NHC}$ -functionalized GC, both of which showed loss of the $\text{C}\equiv\text{C}$ stretch following clicking, albeit with lesser signal intensity (Fig. 3c and d).

In contrast, a control experiment with $^{i\text{Pr}}\text{NHC}$ on steel showed no peak around 2130 cm^{-1} due to its lack of alkyne moiety (Fig. 3b).

Electrochemical SHINERS (EC-SHINERS)

Having demonstrated the effectiveness of SHINERS to amplify and detect the presence of alkyne moieties in the NHC coating, we next applied this method *in situ* to gain mechanistic insight into the deposition process by monitoring changes in the alkyne peak. Given the stronger Raman signal observed for $^{Di\text{-Alk}}\text{NHC}$



on steel, we focused our investigation on this system. In these experiments, SHINs were first deposited onto a steel substrate. The laser was then focused on the surface, while a potential was applied to the steel electrode, which was submerged in a solution containing the NHC precursor (see Fig. S2 for a photograph of the experimental setup). Raman spectra were recorded every 25 seconds over the course of \sim 10 minutes (Fig. 3e). The full spectral range is available in Fig. S15 of the SI.

At open circuit potential (OCP), the characteristic signal of $\text{C}\equiv\text{C}$ stretch at 2133 cm^{-1} is detectable due to the presence of $^{\text{Di-Alk}}\text{NHC}$ precursor in the solution. Upon applying a potential of -1.2 V , immediate spectral changes occurred: a transient peak at 2050 cm^{-1} appeared and decayed within \sim 4 minutes, and a stable peak emerged at 2103 cm^{-1} . Shifting of the $\text{C}\equiv\text{C}$ stretch toward lower frequencies suggests a weakening of the triple bond. The peak at 2050 cm^{-1} coincides with the characteristic range for iron acetylides ($\nu(\text{C}\equiv\text{C-Fe}) = 2040\text{--}2060\text{ cm}^{-1}$),⁵⁵ suggesting that alkyne may interact with Fe ions leaching from the steel surface. The 2103 cm^{-1} peak closely matches the reported value for Pt acetylides ($\nu(\text{C}\equiv\text{C-Pt}) = 2104\text{ cm}^{-1}$),⁵⁶ indicating a potential dissolution of the Pt counter electrode as well; a consequence of our electrochemical setup. Overall, the *in situ* detection of metal acetylide species is consistent with the mechanism of acetylide-initiated polymerization that was proposed by Berg *et al.*²⁹ for alkyne-functionalized NHC, as depicted in Scheme 1. After washing and drying, the acetylides likely reacts with available H^+ to regenerate the alkyne, which explains why the peak at 2133 cm^{-1} is detected on the dried surface (Fig. 3a).

Fig. 3e shows a similar EC-SHINERS experiment, this time conducted during the e-click step. A freshly prepared sample of $^{\text{Di-Alk}}\text{NHC}$ -functionalized steel was coated with SHINs and immersed in a solution containing Cu^{II} (0.1 mM), as well as azide ($\text{N}_3\text{-PEG}_4\text{-biotin}$, 1.75 mM) and supporting electrolyte (50 mM NBu_4PF_6). A potential of -0.2 V was applied for 10 minutes, during which the $\text{C}\equiv\text{C}$ peak of $^{\text{Di-Alk}}\text{NHC}$ at 2133 cm^{-1} gradually decreased. Within approximately 8 minutes, the signal was almost completely lost, indicating the completion of the cycloaddition reaction within this timeframe. Interestingly, under these conditions, metal acetylide formation is suppressed, suggesting that it does not occur at low potentials.

Fluorescence mapping

The ability to attach molecules to surfaces prompted us to use fluorescence measurements to visualize the surface coverage of electrodeposited NHC films. First, the NHCs were electrodeposited onto the substrate of interest, followed by the attachment of $\text{N}_3\text{-PEG}_4\text{-biotin}$ *via* CuAAC using sodium

ascorbate (NaAsc) reduction (Fig. 4a). Capitalizing on the well-established biotin-streptavidin interaction,^{42,57} a fluorescent dye-streptavidin conjugate (Fluor-SA) was attached to the biotin moiety, and the samples were examined under a fluorescence microscope.

As shown in the fluorescence maps of Fig. 4b, emission was detected for NHC-deposited areas on both GC and Cu. For steel, corrosion was visually observed after incubation with Fluor-SA which led to physisorption of the dye, making the method unsuitable for this substrate. A control experiment with $^{\text{iPr}}\text{NHC}$ demonstrated that the triple bond is required for the attachment of FluorSA conjugate, excluding possible weak interactions between the dye and the NHC coatings. For Cu, we found that both $^{\text{iPr}}\text{NHC}^{\text{Alk}}$ and $^{\text{Di-Alk}}\text{NHC}$ enabled clear detection of a fluorescent coating, consistent with the well-documented interaction between various NHCs and copper substrates.^{12,24,26,58}

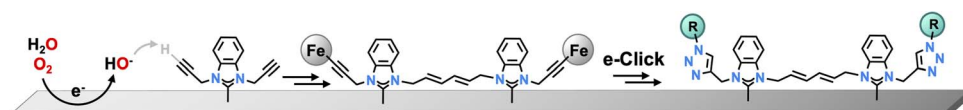
Interestingly, inhomogeneities were observed by the presence of several defects on Cu, likely formed during the electrochemical deposition process.

For GC, only $^{\text{Di-Alk}}\text{NHC}$ produced a detectable signal. We hypothesize that this is due to $^{\text{Di-Alk}}\text{NHC}$ ability to undergo polymerization, facilitated by the presence of two alkyne groups instead of one. XPS analysis of the GC substrates revealed the presence of supporting electrolyte (K^+ or Na^+ , depending on whether KPF_6 or NaI was used), which could not be removed by washing in an ultrasonic bath, suggesting that the electrolyte becomes trapped in the NHC multilayer (see Fig. S19 and S20, SI).

Diazoniums vs. NHCs

The ability of $^{\text{Di-Alk}}\text{NHC}$ to form a resistant coating on GC makes them comparable to diazonium salts, which are often used to functionalize various carbon surfaces.^{59,60} Like NHCs, diazonium salts can be deposited *via* electrochemical reduction and form covalent bond with metals or carbon, but in the case of diazonium salts, this process occurs *via* the formation of reactive aryl radicals.^{61,62} Fig. 4b shows the surface map obtained when 4-ethynylbenzene-1-diazonium hexafluorophosphate ($^{\text{Alk}}\text{Diazonium}$) was used as the anchor instead of $^{\text{Di-Alk}}\text{NHC}$. Qualitatively, functionalization with the diazonium salt provided a brighter signal, suggesting a greater degree of functionalization. However, the fluorescence signal proved too unstable to quantify, prompting us to turn to XPS analysis.

In these experiments, GC was used as the substrate, and the compounds of interest were electrodeposited. The resulting diazonium and NHC coatings were then tagged by electro-clicking with a silane ($\text{N}_3\text{-PEG}_3\text{-Si(OEt)}_3$), enabling detection



Scheme 1 Proposed scheme for the acetylide-initiated electro-polymerization of $^{\text{Di-Alk}}\text{NHC}$ (similar to Berg *et al.*²⁹). Continuation could lead to longer chain.



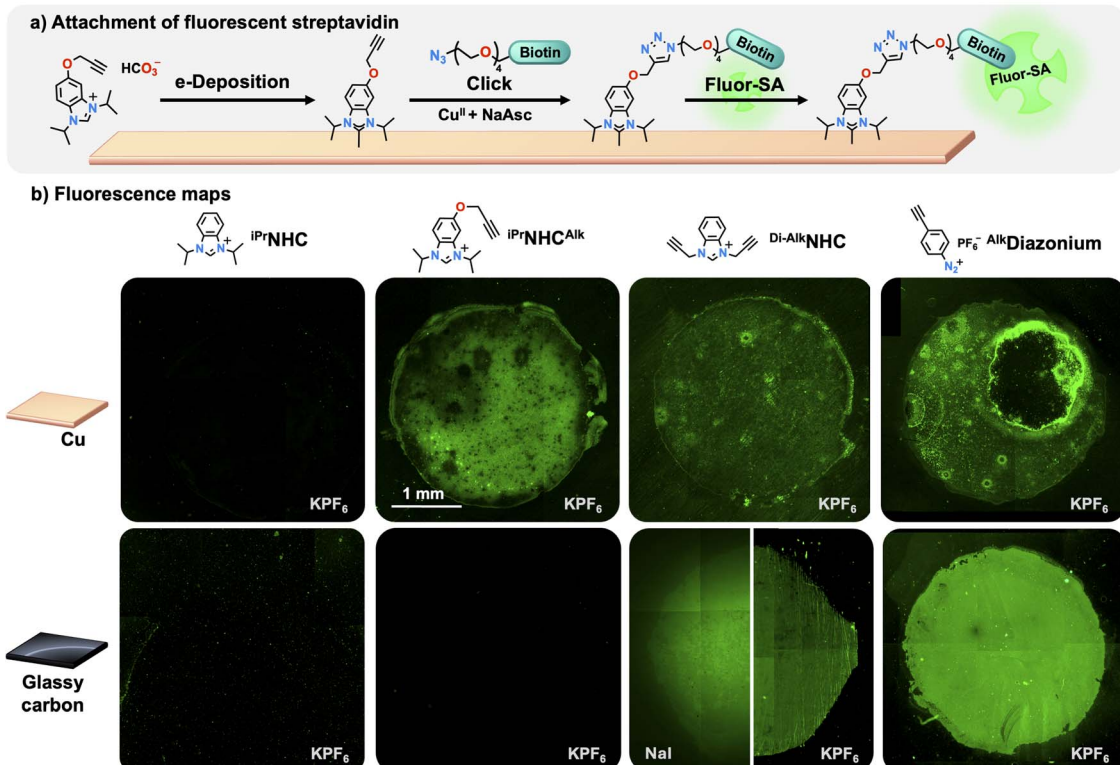


Fig. 4 (a) Schematic representation of surface modification using NHCs and a dye-streptavidin conjugate. (b) Resulting fluorescence maps. The surfaces were electrodeposited with NHCs or diazonium salts (10 mM) followed by click reaction with $\text{N}_3\text{-PEG}_4\text{-biotin}$ and conjugation to green fluorophore-labeled streptavidin. Electrodeposition was performed in CH_3CN with KPF_6 or NaI (50 mM) as supporting electrolytes. The electrochemical deposition was restricted to a 3 mm diameter circle.

via Si 2p XPS. In a control experiment, a glassy carbon sample underwent the same electro-click procedure without prior deposition of diazonium or NHC. Fig. 5a presents the recorded Si 2p signal for these surfaces, while Fig. 5b shows the corresponding atomic percent obtained from survey scans. These

results indicate that the amount of silane clicked onto the surface was 2.4 times greater when using AlkDiazonium compared to Di-AlkNHC , despite the latter containing twice the number of alkyne groups.

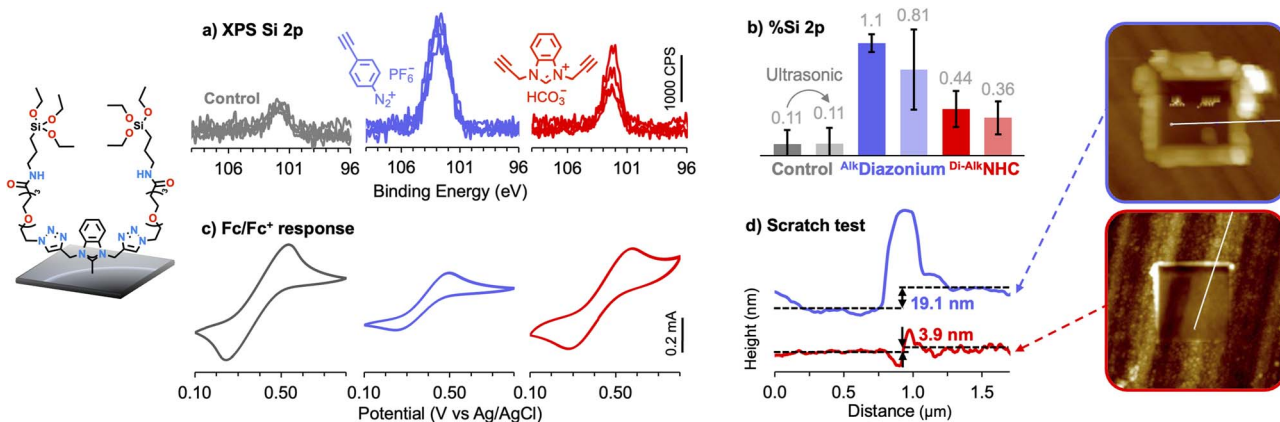


Fig. 5 (a) Comparison of Si 2p signals for surfaces functionalized with a Si-tagged azide using either diazonium or Di-AlkNHC anchoring. The control was treated with the azide without prior deposition of an anchor molecule. (b) Si 2p atomic percentages from survey spectra before and after 15 min sonication in a 1:1 $\text{CH}_3\text{CN}/\text{H}_2\text{O}$ mixture; error bars represent one standard deviation from four independent measurements per sample. (c) CVs for GC electrodes coated from 10 mM Di-AlkNHC or AlkDiazonium solutions, recorded in 10 mM ferrocene in CH_3CN with 50 mM NBu_4PF_6 at a scan rate of 200 mV s⁻¹ per day) AFM scratch tests and corresponding depth profiles for AlkDiazonium - and Di-AlkNHC -functionalized GC substrates.

To assess the durability of the coatings, the same samples were then subjected to cleaning in an ultrasonic bath for 15 minutes using a 50 : 50 mixture of H_2O and CH_3CN . In terms of relative values, $^{\text{Alk}}\text{Diazonium}$ and $^{\text{Di-Alk}}\text{NHC}$ showed similar desorption, and therefore more silane remained on the surface when using $^{\text{Alk}}\text{Diazonium}$ anchor.

The superior surface coverage of diazonium is consistent with expectations, given that diazonium salts are known to form thick multilayers (6–15 nm).^{63,64} In contrast, NHCs are known to form monolayers (~ 0.8 nm),⁶⁵ or in the case of polymerizable alkyne-NHC, thin multilayers (2.0 nm).²⁹ The formation of multilayers when using anchor molecules is associated with passivation of the substrate and results in a disordered surface.⁶⁶ For the design of electrochemical sensors, this insulating layer is synonymous with loss of the redox signal, and thus, detrimental to the performance of the device.

To compare the passivation caused by diazonium and NHC coatings, we e-deposited each anchor on a GC electrode and recorded the redox signal of the ferrocene/ferrocenium couple (Fig. 5c). The signal obtained using a clean, freshly polished GC electrode is also shown in grey. As expected for the thinner

coating, NHC showed less passivation, while the diazonium coating hindered charge transfer. Specifically, passivation of the electrode led to a reduction in anodic peak current of 32% for the diazonium, and 14% for NHC. A similar trend was observed when using a Pt electrode, but the contrast was even more pronounced; the anodic peak current for diazonium reduced by 70% versus only 15% for NHC after passivation of Pt (Fig. S8, SI).

Differences in film thickness were confirmed by AFM scratch tests performed on $^{\text{Alk}}\text{diazonium}$ - and $^{\text{Di-Alk}}\text{NHC}$ -modified glassy carbon surfaces (Fig. 5d). The diazonium film was measured as ~ 19 nm, consistent with the formation of thick multilayers. In contrast, $^{\text{Di-Alk}}\text{NHC}$ film was found to be ~ 4 nm thick. Considering that the precursor is approximately 6.6 Å in length, this corresponds to approximately six layers. To reduce the inherent passivation caused by diazonium-derived films, efforts have been made in the literature to form diazonium monolayers. For example, protection of the alkyne moiety using bulky triisopropylsilyl (TIPS) protecting groups have been shown to hinder aryl radical grafting, leading to a 0.65 nm thick monolayer.⁶³ In contrast, the ability of $^{\text{Di-Alk}}\text{NHC}$ to deposit in self-limited 4 nm layers without the need for protection or

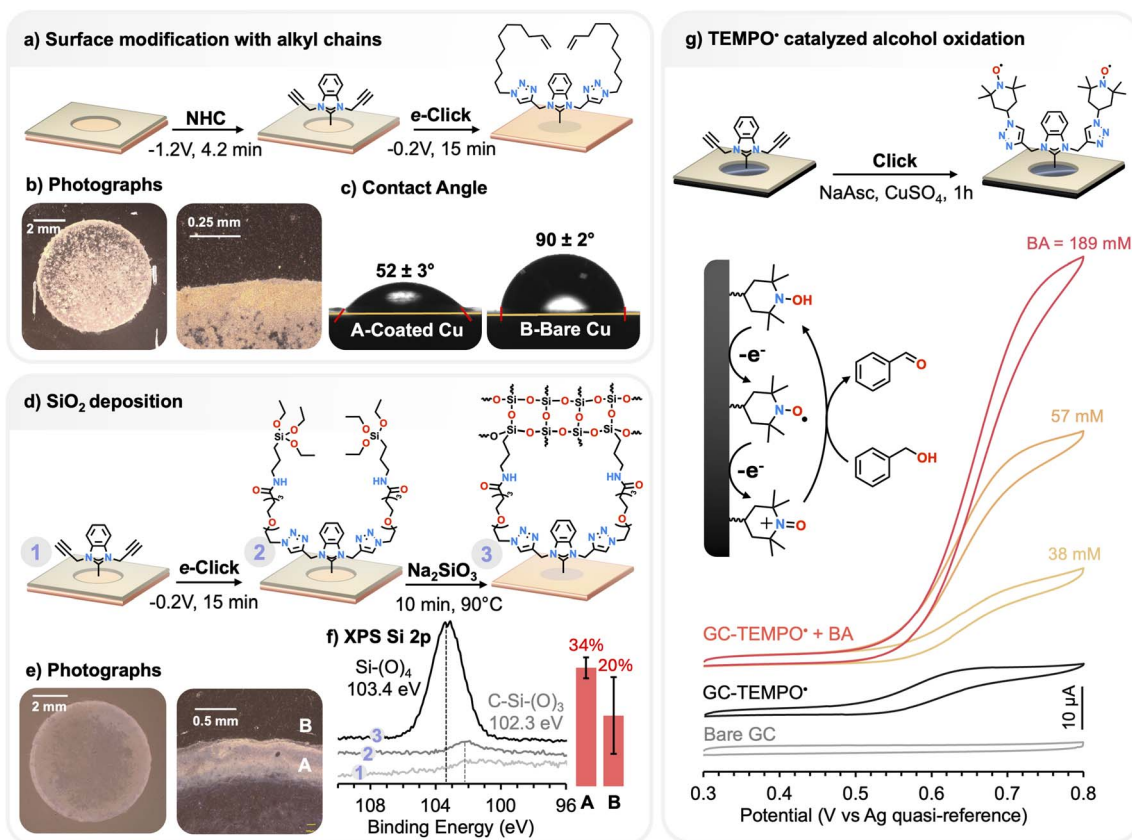


Fig. 6 Exploration of NHC-based surface modification. (a) Functionalization of a copper surface with alkyl chains. (b) Photographs of the modified surface, showing the functionalized area and a close-up view. (c) Contact angle measurements for the surface outside and within the modified region; data shown corresponds to one of three drops analyzed. (d) Functionalization of a copper surface with SiO_2 . (e) Photographs. (f) XPS Si 2p signal for the bare surface (label "1"), the surface after NHC modification and clicking with $\text{N}_3\text{-PEG}_3\text{-Si(OEt)}_3$ (label "2"), and the final surface after silica growth (label "3"). The bar graph shows the Si signal measured by survey XPS inside and outside the NHC-modified region, showing a superior Si coverage inside the NHC-modified area. Error bars represent one standard deviation, for 10 points analyzed on the surface. (g) Functionalization of glassy carbon with the persistent radical TEMPO*, followed by electrochemical analysis of its response to increasing concentrations of benzyl alcohol (BA). Obtained at a scan rate of 50 mV s⁻¹ in aqueous carbonate buffer (pH 10.0).



deprotection steps, as demonstrated here, may presents an advantage over diazonium-based multilayers.

Surface modifications

As a proof of concept for the use of NHCs as molecular anchor, we examined the breadth of surface modifications possible. Considering that ^{Di-Alk}NHC showed the greater degree of functionalization in the F 1s experiments, we focused on this compound. ^{Di-Alk}NHC was e-deposited onto copper in a 7 mm diameter circular area and subsequently e-clicked with 11-azidoundec-1-ene. As seen in Fig. 6b, a simple visual inspection clearly shows material deposition in the region of interest. This was further confirmed by contact angle measurements, which showed a large increase in wettability. Specifically, the water contact angle of the bare surface decreased from $90 \pm 2^\circ$ to $52 \pm 3^\circ$ after deposition. A control experiment, where the surface was treated with 11-azidoundec-1-ene without prior NHC anchoring, showed no change in wettability relative to bare copper ($87 \pm 2^\circ$), confirming the necessity of NHC for anchoring.

In a second demonstration, ^{Di-Alk}NHC was e-deposited on a copper surface and silanized *via* e-click using N_3 -PEG₃-Si(OEt)₃. Sodium silicate was then used to grow an SiO₂ layer from the surface. Fig. 6e shows photographs of the modified surface, while Fig. 6f presents the corresponding XPS Si 2p signal. A small peak at 102.3 eV is observed after the clicking step, consistent with the presence of $-C-Si(OEt)_3$.⁶⁷ Following the growth process, the Si signal is dominated by a new peak at 103.4 eV, indicative of the formation of a thick SiO₂ overlayer.⁶⁷ Because silicate can bind by itself to copper, a region outside the NHC-functionalized area was analyzed as a control. While the control area also shows the presence of SiO₂, its amount on the surface appears lower, and its distribution less homogenous compared to the ^{Di-Alk}NHC-modified region. These results highlight a slight advantage of using NHC anchoring as a pretreatment for silica deposition.

The third demonstration involved the immobilization of an electrochemically active catalyst on GC. This approach is used for heterogeneous catalysis which improves recyclability and reduces chemical waste relative to homogeneous reactions, because the functionalized electrode can easily be reused. Specifically, the immobilization of the persistent radical TEMPO[·] (2,2,6,6-tetramethylpiperidine 1-oxyl) was investigated due to its well-established role in the chemoselective oxidation of alcohols to their corresponding ketones or aldehydes.⁶⁸⁻⁷⁰ This process begins with the anodic oxidation of TEMPO[·] to its oxoammonium cation (TEMPO⁺), which, under basic conditions, reacts with primary and secondary alcohols *via* formation of alkoxide adducts. Various anchoring strategies have been explored to enable the use of TEMPO[·] in heterogeneous catalysis, including amide-,⁷¹ thiol-,⁷² and silatrane-based⁷³ linkages. Fig. 6g presents the CVs obtained for a similarly TEMPO[·]-functionalized electrode but using ^{Di-Alk}NHC as the anchor molecule. The CVs were obtained in aqueous carbonate buffer at pH 10.0.

A small but discernible redox signal could be observed and is consistent with the presence of TEMPO[·]/TEMPO⁺ couple

(Fig. 6g, black trace).^{73,74} Upon addition of benzyl alcohol (BA), the signal became sigmoidal and irreversible, accompanied by an increase in anodic peak current (Fig. 6g, red and yellow trace). This behaviour is characteristic of TEMPO[·]-catalyzed alcohol oxidation systems,^{73,74} and the current increase reflects both the substrate concentration and TEMPO[·]'s catalytic turnover on the timescale of the CV.⁶⁹ Importantly, the TEMPO[·] signal persisted after reusing the electrode for another experiment, demonstrating that the NHC remained immobilized to the electrode (see Fig. S11, SI). However, CVs analysis performed at different scan rate revealed a high capacitive current which made extraction of the anodic and cathodic peak current impossible (Fig. S10). This limitation indicates a potential area for improvement in applications such as biosensors.

Conclusion

In summary, this work demonstrates that NHCs containing alkyne moieties can effectively attach to various substrates and enable surface functionalization *via* click chemistry. These molecules are therefore viable molecular anchors compatible with a wide range of surfaces, including copper, low carbon steel and glassy carbon. Despite the reported desorption of NHCs at low negative potential,^{40,75} electrochemical reduction was found to be both fast and efficient for NHC deposition and clicking. *In situ* Raman monitoring showed that deposition proceeded *via* the formation of metal acetylides, providing further evidence for an acetylide-initiated polymerization mechanism.²⁹ Additionally, the electro-click reaction was found to complete within 8 minutes.

The ability of NHCs to firmly attach to surfaces, confirmed by sonication tests, reinforces their potential as a promising alternative to thiol monolayers for surface functionalization. When compared to diazonium salts, XPS and fluorescence experiments showed that ^{Di-Alk}NHC provided lower surface coverage, resulting in less material attached to the surface. The formation of a thinner multi-layer offered an advantage for NHCs: a smaller barrier to charge transfer. We believe this inherent conductivity, combined with NHC's ability to form robust covalent bond, could facilitate the design of more durable electrochemical devices, as exemplified by the immobilization of the TEMPO[·] catalyst on an electrode.

Experimental

Materials

Low carbon steel sheets (1 mm thickness) were obtained from SSAB (Stockholm, Sweden) and contained >99.5 wt% Fe and 0.053 wt% C. The full elemental composition is available in Table S1 of the SI. Glassy carbon plates (1 mm thickness) were obtained from ThermoFisher Scientific. Copper sheets (1 mm thickness) were obtained from GoodFellow Cambridge (Huntingdon, United Kingdom). The substrates were polished using grinding foils and pads from Struers, including silicon carbide grinding foils with grit sizes P320, P1200, and P4000, along with their MD-Pan, MD-Mol, and MD-Nap polishing pads.

The electrochemical cell used for Raman measurements was obtained from *Redox.me* (SKU: C-O-RAM_SM_ECFC). The cell used for e-deposition and e-clicking was a corrosion cell from the same supplier (SKU: C-O-BMM_CC-15-1).

N_3 -PEG₂₃-N₃, N_3 -PEG₄-biotin and N_3 -PEG₃-Si(OEt)₃ were purchased from *BroadPharm* (San Diego, CA, USA) (Catalog # BP-40081, BP-22119 and BP-24073 respectively). 3,5-Bis(trifluoromethyl)benzyl azide (N_3 -benzyl-(CF₃)₂) was obtained from *CF Plus Chemicals*. Streptavidin, Alexa FluorTM 488 Conjugate (Fluor-SA) was purchased from *ThermoFisher Scientific* (2 mg mL⁻¹, Catalog #S32354). Bovin serum albumine was purchased from *BioBasic* (Markham, Ontario, Canada). Gold chloride trihydrate (HAuCl₄·3H₂O, >99.9% purity), (3-amino-propyl)trimethoxysilane (9% purity), sodium silicate solution 27% (Catalog # 338443), tetrabutylammonium hexafluorophosphate (NBu₄PF₆, >99.0% purity), potassium hexafluorophosphate (KPF₆, 99.5% purity) and tris(3-hydroxypropyltriaziolylmethyl)amine (95%) were purchased from *Millipore Sigma*. Sodium iodide (NaI, ACS grade) and (+)-sodium-L-ascorbate crystalline (NaAsc) were purchased from *Oakwood Chemical*. Copper(II) sulfate pentahydrate (CuSO₄·5H₂O, >99% purity) was purchased from *Acros Organics*. N_3 -TEMPO[·] and benzylalcohol were purchased from *MedChemExpress* (Monmouth, NJ, USA).

Electrochemical sample masks were obtained from *Gamry Instruments* (Warminster, USA) and hole-punched to the desired circumference. HPLC-grade CH₃CN, and MeOH as well as ACS-grade acetone were purchased from *ThermoFisher Chemicals*. EtOH was obtained from *Commercial Alcohols* (Ontario, Canada). All reagents were used as received without further purification.

Pre-treatment of the copper, steel and glassy carbon substrates

Glassy carbon squares of 1.5 × 1.5 cm² were polished using 0.05 µm alumina suspension and then activated by performing 25 consecutive CV scans in 0.1 M aqueous H₂SO₄ at a scan rate of 50 mV s⁻¹, with a potential range of -0.2 to 2.2 V *versus* an Ag wire quasi-reference electrode. This anodization process introduces functional groups (e.g. C=O) to the surface and enhance reproducibility in electrochemical methods.^{76,77} In our case, it led to an improvement of surface coverage of the NHC (see Section 7 of the SI for more details).

For experiments on steel and copper, the pre-treatment involved polishing the samples to a mirror-like finish. This was achieved using a *Struers TegraForce-5* polishing machine with sequential 3 minutes polishing using various polishing pads, from coarse to fine. Silicon carbide grinding foils with grit size of P1200 and P4000 were used, followed by polishing with MD-Pan, MD-Mol, and MD-Nap pads using diamond suspensions of 9, 3, and 1 µm, respectively. The polished samples were then cleaned by sonication in acetone and isopropyl alcohol. To minimize corrosion, the samples were used within three days of polishing.

Scanning Electron Microscopy (SEM) images of the polished and activated surface are included in the SI (Fig. S5) and show all surfaces to be relatively smooth on the 50 µm scale.

For *in situ* SHINERS measurements, the samples were polished to a coarser finish (P4000), resulting in a visibly matte surface.

Synthesis of the NHC precursors (imidazolium carbonate salts)

Compounds 1,3-diisopropyl-1*H*-benzo[*d*]imidazole-3-ium hydrogen carbonate (ⁱPrNHC), 1,3-diisopropyl-6-(prop-2-yn-1-yloxy)-1*H* benzo[*d*]imidazole-3-ium hydrogen carbonate (ⁱPrNH-C^{Alk}) and 1,3-di(prop-2-yn-1-yl)-1*H*-benzo[*d*]imidazole-3-ium hydrogen carbonate (^{Di-Alk}NHC) were synthesized according to the procedures published by Crudden *et al.*,¹¹ S. G. Selva *et al.*³¹ and Jiang *et al.*,¹² respectively. FTIR spectra, ¹H-NMR and ¹³C-NMR are provided in Section 14 of the SI.

Synthesis of ^{Alk}Diazonium·PF₆⁻, 11-azidoundec-1-ene and 1-azidohexane

4-Ethynylbenzenediazonium hexafluorophosphate (^{Alk}Diazonium·PF₆⁻) was synthesized according to the method reported by Zhang *et al.*⁷⁸ 11-Azidoundec-1-ene and 1-azido-hexane were synthesized according to procedure published by Sinha *et al.*⁷⁹

SHINs synthesis

SHINs were synthesized following the detailed protocol reported by Li *et al.*⁵⁴ The procedure is designed to yield AuNPs with a diameter of 55 nm; the particles synthesized herein had a diameter of ~52 nm, as determined by their plasmon band at 535 nm⁸⁰ (Fig. S14). The thickness of the silica shell is dictated by the time spent in the silicate solution. We used a growth time of 20 minutes at 90 °C, which has been reported to produce 2 nm SiO₂ layer.⁵⁴ The SHINs were stored at room temperature in the dark until Raman experiments, for up to ~3 weeks.

Electrodeposition of NHCs on low carbon steel, copper, and glassy carbon

Deposition was achieved by adding the NHC precursor (0.025 mmol, 5 mM, unless otherwise noted) and supporting 50 mM electrolyte (NaI, NBu₄PF₆, or KPF₆, as specified in the respective section) to a 5 mL volumetric flask. To this flask, 5 µL of distilled H₂O was added as a source of ROS, similar to previously published methods.⁴⁶ The flask was filled to 5 mL with CH₃CN, leading to a total content of 0.1% v/v H₂O in CH₃CN. The solution was *not* degassed to allow the formation superoxide (O₂^{·-}) and ROS at the working electrode. The solution was then added to the electrochemical cell, in which the working electrode consisted of the substrate of interest (copper, low carbon steel, or glassy carbon plate cut to 1.5 × 1.5 cm²) covered by hole-punched insulating sample mask to restrict the deposition to a specific area. The counter electrode was a Pt coil, and an Ag wire was used as quasi-reference electrode. A photograph of the setup is available in Fig. S1 of the SI. Deposition was achieved by applying 25 pulses of 5 seconds at a potential of -1.2 V, each followed by 5 seconds of relaxation. The total duration of the deposition was therefore 4 minutes



and 10 seconds. The potential of -1.2 V was selected based on previously reported methods.⁴⁶ A *Vionic* potentiostat (Metrohm, Florida, USA) was used. An example of the chronoamperogram obtained during deposition is presented in the SI (Fig. S3). After deposition, the cell was disassembled, and the insulating sample mask was kept on the surface for the next step (e-click). The samples were washed by submerging them in approximately 5 mL of H_2O , followed by 5 mL of CH_3CN , and then rinsed with EtOH; some were also cleaned by sonication, as indicated in the text.

Electrodeposition of $^{\text{Alk}}$ Diazonium

$^{\text{Alk}}$ Diazonium was deposited by performing 6 consecutive CV scans between potentials of 0 and -1.0 V at a scan rate of 50 mV s^{-1} . To ensure a fair comparison with NHC, the same electrochemical setup, sample pretreatment, anchor concentration, electrolyte composition, and rinsing methods were used. Both the NHC and diazonium samples were prepared and analyzed on the same day. The current response observed during the electrodeposition of $^{\text{Alk}}$ Diazonium on the activated glassy carbon surface showed the typical pattern attributed to passivation, as presented in Fig. S7 of the SI.

Electro-clicking

A solution containing the azide (1–20 mM, see respective section) and NBu_4PF_6 (96.9 mg, 0.25 mmol, 50 mM) in CH_3CN was prepared in a 5 mL volumetric flask. NaI could not be used for the click reaction, because it reacted with CuSO_4 . To the flask, 10 μL of a stock solution of CuSO_4 was added, resulting in a final concentration of 64 μM Cu^{II} . Reduction to Cu^{I} was achieved by applying a potential of -0.2 V for 15 minutes, similar to a previous report for e-click with $^{\text{Alk}}$ Diazonium.⁴⁹ An example of the chronoamperogram obtained during clicking is presented in Fig. S4 of the SI. After the reaction, the insulating sample mask was carefully removed, and the samples were washed by submerging them in H_2O and CH_3CN , then rinsed with EtOH. Electro-clicking on GC was problematic, because the electrolyte could not be removed by sonication (as detected by XPS), presumably due to the material's porous structure. As a result, chemical clicking using NaAsc as the reducing agent proved advantageous to obtain a clean surface.

Non-electrochemical functionalization (immersion method)

The immersion method was performed by placing steel or copper samples in a 5 mM solution of $^{\text{Di-Alk}}$ NHC in MeOH, in a covered beaker, and leaving them undisturbed at room temperature for 66 hours. This procedure follows previously reported methods.^{11,28} After deposition, the samples were sequentially rinsed with water, acetonitrile, and ethanol to remove physisorbed NHC species. For the click reaction, 50 μL of a freshly prepared stock solution containing 2.6 mM CuSO_4 , 3.5 mM tris(3-hydroxypropyltriazolylmethyl)amine, 23 mM sodium ascorbate, and 320 mM $\text{N}_3\text{-benzyl-(CF}_3\text{)}_2$ was applied to the substrate and allowed to react in the dark for 1 hour. Following the reaction, the samples were cleaned using the

same procedure as the electrochemical method, sonicating them for 10 minutes in a 1 : 1 mixture of acetonitrile and water.

Fluorescence images

Samples were prepared using the previously described pretreatment and e-deposition method, from solutions of NHC or diazonium salts (10 mM) with KPF_6 or NaI as the supporting electrolyte. The surfaces were then rinsed three times with Milli-Q water and dried with an air flow. For fluorescence mapping, the click reaction was achieved chemically rather than electrochemically to reduce the amount of $\text{N}_3\text{-PEG}_4\text{-biotin}$ used because it requires as little as 90 μL to fully cover the NHC-functionalized region. This was accomplished by preparing a solution containing $\text{N}_3\text{-PEG}_4\text{-biotin}$ (3.5 mg, 7.16 μmol , 80 mM), CuSO_4 (1.17 mM), the click-accelerating ligand tris(3-hydroxypropyltriazolylmethyl)amine (2.5 mM), and NaAsc (16.7 mM) in 90 μL of a mixture of 83% v/v Milli-Q H_2O and 17% v/v MeOH. The solution was carefully dropped on the substrate, ensuring complete coverage of the functionalized area. The substrate was then covered with aluminum foil to protect it from the light and allowed to react for 1 hour at room temperature. Following the reaction, the surface was rinsed with Milli-Q water.

Fluor-SA was attached to the biotin by mixing equal parts of the streptavidin (2 mg mL^{-1} , as purchased) with 3% wt. bovine serum albumin in Milli-Q water, resulting in a dissolution of 1 mg mL^{-1} of Fluor-SA. This mixture was dropped onto the sample and let to react at room temperature and in the dark for 1 hour. The sample was then cleaned by rinsing thoroughly with Milli-Q water.

Fluorescence images were recorded with a *Zeiss Axio Imager 2* fluorescence microscope, using a 5 \times objectives. The samples were kept wet in Milli-Q water, under a coverslip. To visualize the full areas, nine images were stitched together using the *Zeiss' Zen* software. We found that the fluorescence fluctuated over time, which caused vertical and horizontal artefact in the final images, as seen in Fig. 4. The *Axio* microscope is equipped with a *Zeiss* lighting unit (HXP 120C); its emission was filtered by a *Zeiss* filter (Filter set HE 38) which is compatible with Alexa Fluor 488. Specifically, it contains an excitation band-pass filter centered at 470 nm with a bandwidth of 40 nm, a 495 nm beam splitter, and an emission filter centered at 525 nm with a bandwidth of 50 nm.

XPS measurements and fitting

XPS measurements of the surfaces were performed using a *Thermo Fisher Scientific* K-Alpha X-ray photoelectron spectrometer equipped with a monochromatic Al $K\alpha$ source, at McGill University. High-resolution spectra were collected using a spot size of 400 μm , a 0.1 eV step size, and a 50 eV pass energy, while survey spectra were collected with 1 eV step size and 200 eV pass energy. The software *CasaXPS* (version 2.3.26)⁸¹ was used for fitting and analysis. Spectra were charge-corrected to a binding energy of 284.8 eV using the aliphatic peak for adventitious carbon (C 1s).⁸² The peaks in the high-resolution spectra were fitted using the Shirley background function, and



Gaussian–Lorentzian (GL(30)). All N 1s peaks within a sample were fitted using the same full width at half maximum (FWHM).

SHINERS of the functionalized surfaces

The NHC-functionalized sample was prepared following the general electrodeposition procedure, using a solution of NHC of 10 mM. For ^{Di-Alk}NHC, ^{iPr}NHC and ^{iPr}NHC^{Alk} on steel, NBu₄PF₆ (50 mM) was used as electrolyte. For ^{Di-Alk}NHC on GC, KPF₆ (50 mM) was used. After deposition, the sample were washed by immersion in CH₃CN and rinsing with EtOH. Next, 10–30 μ L of aqueous SHINs concentrate was deposited onto the sample, and water was evaporated under vacuum. For ^{Di-Alk}NHC on steel, the sample was clicked electrochemically with N₃-PEG₂₃-N₃ according to the general method. For ^{iPr}NHC^{Alk} on steel, ^{iPr}NHC on steel, and ^{Di-Alk}NHC on GC, the clicking reaction was performed chemically by applying a solution of aqueous CuSO₄ (6 mM) and NaAsc (12 mM) with an excess of the azide and allowing it to react for 10 minutes. The Raman spectra were recorded using a Renishaw inVia Raman microscope, equipped with a 50 \times objective, a 785 nm excitation laser, and a 1200 1 mm⁻¹ grating. Cosmic rays were removed by taking the median of multiple spectra. The laser was focused on both SHINs-coated and non-coated regions. Spectra obtained for non-coated areas (labeled “normal” Raman in Fig. 3a) showed no detectable signal, as there was no plasmonic enhancement from the nanoparticles. In contrast, focusing the laser on SHINs-coated regions produced a clear Raman signal. It is noteworthy to emphasize that SHINERS is non-quantitative due to the inhomogeneous coating of the AuNPs, which results in inconsistent signal amplification. A control experiment, in which SHINs were deposited onto a clean glass substrate, revealed weak signals from the SHINs themselves (Fig. S12, SI) but no peaks in the 1700–2800 cm⁻¹ range which was used to detect the C≡C stretch.

EC-SHINERS

In situ measurements were carried out using a fluorescence/Raman electrochemical cell (see Materials section). A photograph of the setup is shown in Fig. S2 of the SI. A two-electrode configuration was used, with a platinum wire as the counter electrode and the steel substrate as the working electrode. The electroactive area of the working electrode was constrained to a 7 mm diameter hole using an insulating sample mask. Current was applied using a portable potentiostat (*EmStat, PalmSens*). Raman spectra were first recorded at the open-circuit potential (OCP), followed by the application of a −1.2 V potential. Spectra were collected using a *WITec alpha300R* confocal Raman microscope (*Oxford Instruments*, Ulm, Germany) equipped with a *Zeiss* 50 \times objective and a 785 nm laser source. The spectra obtained *in situ* were smoothed using the smoothing function in Renishaw's *WiRE* software to reduce noise, and cosmic rays were removed with the software's automatic correction feature.

To rule out interaction between the NHC and the SHINs, a SHINs-coated glass slide was submerged in a 5 mM solution

of ^{Di-Alk}NHC for 20 hours, rinsed, and analyzed, revealing no detectable triple-bond signal around 2133 cm⁻¹ (Fig. S13).

Surface modification of a copper substrate with 11-azidoundec-1-ene

NHC was deposited onto a 7 mm diameter area of copper using the method described herein, from a 5 mM solution of ^{Di-Alk}NHC with 50 mM NaI as supporting electrolyte in CH₃CN (+0.1% v/v H₂O). After washing, the sample underwent electro-clicking with a solution of 20 mM 11-azidoundec-1-ene, 50 mM NBu₄PF₆, and 64 μ M CuSO₄ in CH₃CN. A control sample, treated identically with 11-azidoundec-1-ene but without prior NHC treatment, showed no visible deposit and no change in the contact angle measurement (87 \pm 2°) relative to bare copper surface (90 \pm 2°), indicating that 11-azidoundec-1-ene does not interact with copper on its own (see Fig. S23 for all contact angle measurements).

Silanization and SiO₂ growth on the copper surface

NHC was deposited onto a 7 mm diameter area of copper using the described deposition method, from a 5 mM solution of ^{Di-Alk}NHC with NaI as a supporting electrolyte in CH₃CN (+0.1% v/v H₂O). Silanization was then performed using the electro-click method, from a solution of 1.0 mM N₃-PEG₃-Si(OEt)₃ in CH₃CN with 50 mM NBu₄PF₆ and 64 μ M CuSO₄. After the click reaction, the sample was rinsed with H₂O, CH₃CN, and EtOH, then immersed in a beaker containing 10 mL of Milli-Q water at 90 °C. One mL of an aqueous sodium silicate solution (0.54% wt/wt, adjusted to pH ~10 using HCl, prepared from 27% wt/wt sodium silicate) was added, and the SiO₂ layer was allowed to grow for 15 minutes at 90 °C. The sample was then removed and cleaned by sonication in H₂O for 1 minute. Presence of the electrolyte NaI was found to be below the limit of detection by survey XPS scans (see Fig. S21, SI).

Cyclic voltammetry in ferrocene

A glassy carbon electrode (*CH Instrument*, Texas, USA) was activated in H₂SO₄ using the method described in the pre-treatment section. ^{Alk}Diazonium or ^{Di-Alk}NHC were then deposited onto the GC electrode from precursor solutions of 10 mM in CH₃CN and 50 mM NaI. A Pt coil was used as the counter electrode, and an Ag/AgCl electrode was used as the reference. Electrode passivation was assessed by performing CVs in 10 mM ferrocene, at a scan rate of 200 mV s⁻¹, within a potential range of +0.1 to +0.8 V vs. Ag/AgCl. Five scans were done in total; the data shown corresponds to the two last scans. For the control, the same electrode was freshly polished with a 1 μ m alumina suspension.

Density functional theory calculations

All calculations were performed using the *Gaussian 16* software suite.⁸³ XPS binding energies were calculated according to Koopman's theorem, which assumes that the ionization energy of an electron corresponds to the negative of its orbital energy. This method for predicting XPS spectra has been previously



reported and benchmarked, demonstrating reliable accuracy when using the B3LYP functional.⁸⁴ The structure of the imidazolium precursor was modeled as a cation without its HCO_3^- counterion. The NHC bonded to the steel substrate was represented as a single $\text{iPrNHC}^{\text{Alk}}$ molecule bonded to one Fe atom (see SI, Section 15). Geometries were optimized at the B3LYP/6-311+G(2d,2p) level of theory⁸⁵⁻⁸⁸ with the SMD solvation model for EtOH.⁸⁹ The N 1s orbital was located, and the negative of its energy was expressed in electron volts (eV) to estimate the binding energies. Absolute values are typically not accurate, so all values were shifted relative to the benzimidazolium precursor's N 1s peak at 401.12 eV (see the SI of Selva *et al.*³¹ for the XPS of $\text{iPrNHC}^{\text{Alk}}$). Binding energies are therefore expressed as relative shifts from this reference peak.

The vibrational spectrum of Di-AlkNHC was calculated at the B3LYP/6-311+G(2d,2p) level of theory with the SMD solvation model for CH_3CN . The structures were first optimized, and frequency calculations confirmed local minima by the absence of imaginary frequencies. The spectrum was visualized using *GaussView* software, applying an arbitrary full width at half maximum of 4 cm^{-1} . To account for anharmonicity, frequencies were scaled by a factor of 0.98.

Optical images (photographs) of the copper surfaces

Surface imagery was done using a *Keyence VHX-7100* microscope equipped with a 4 K fully integrated head, at McGill University. Samples were washed with EtOH, H_2O and CH_3CN before taking images.

Contact angle measurement

The contact angle measurements were conducted using *Data-Physics OCA 15 EC Optical Contact Angle Instrument* at McGill University. The bare and coated Cu surfaces were analyzed using a 1 μL droplet and images were captured to obtain respective contact angle values. Using Young–Laplace fit, the contact angle values were obtained for the whole droplet. Three droplets were analyzed for each region, and all pictures can be found in the SI (Fig. S23).

TEMPO[·]-catalysed alcohol oxidation

A GC substrate was roughened with P320 grinding foil to increase its surface area and then activated in H_2SO_4 as previously described. Di-AlkNHC was electrochemically deposited on a 3 mm diameter area according to the general method, using a 5 mM NHC solution with 50 mM NaI. After washing, a reaction solution containing CuSO_4 (0.7 mM), tris(3-hydroxypropyltriazolylmethyl)amine (1.0 mM), $\text{N}_3\text{-TEMPO}^{\cdot}$ (69 mM), and NaAsc (3.3 mM) in a solvent mixture (30% v/v H_2O , 17% v/v MeOH, 35% v/v DMSO, 17% v/v CH_3CN) was applied to the surface and allowed to react for one hour. This solvent mixture was used because of the low solubility of $\text{N}_3\text{-TEMPO}^{\cdot}$ in water. The surface was then rinsed with water and EtOH and placed in the electrochemical cell. All measurements were done under aerobic conditions in aqueous buffer at pH 10.0 using a solution of $\text{Na}_2\text{CO}_3/\text{NaHCO}_3$ (50 mM each). Initially, no signal was detected, likely due to the reduction of TEMPO[·] into an

inactive form during the click reaction. Activation of the electrode was achieved by performing two CV scans up to +1.5 V, which restored the reversible TEMPO[·]/TEMPO⁺ redox signal around +0.5 V *vs.* Ag quasi-reference electrode. Next, BA was added directly to the solution, stirred, and CVs were recorded at 50 mV s^{-1} . After the measurements, the cell was disassembled, rinsed with water and CH_3CN , dried, and reassembled. A subsequent CV measurement showed the signal persisted, confirming that TEMPO[·] remained immobilized to the surface during the first analysis (see SI, Fig. S8).

Scratch test using atomic force microscopy (AFM)

Atomic force microscopy (AFM) was carried out under ambient conditions using a Dimension ICON system equipped with an NS VI controller (Bruker, Santa Barbara, CA, USA), at Université de Montréal. Imaging was conducted in PeakForce Tapping mode (PeakForce QNM®) with DNP-A silicon nitride triangular probes (Bruker), featuring a nominal tip radius of 20 nm and a spring constant of 0.58 N m^{-1} . A scratch test was performed over a $1 \times 1 \mu\text{m}$ region by applying a PeakForce setpoint of 200 nN (200 times higher than the imaging setpoint) for 10 minutes at a scan rate of 20 Hz. Afterward, a larger $5 \times 5 \mu\text{m}$ area was imaged to assess the scratched region. Prior to step height analysis, raw height images were processed using a first-order XY Plane Fit followed by a first-order Flatten to remove tilt and background slope, using the Nanoscope Analysis software (version 3.0). Indentation channel images were used to confirm increased stiffness in scratched regions, indicating that the scratched region correspond to glassy carbon.

Author contributions

A. J. contributed to conceptualization, performed synthesis of SHINs and $^{\text{Alk}}$ Diazonium, SHINERS experiments, electrodeposition and click chemistry, DFT calculations, fluorescence measurements, proof-of-concept functionalization, and XPS experiments. A. J. also wrote, edited, and prepared figures for the manuscript. A. N. contributed to conceptualization, XPS fitting, and synthesized 1-azidohexane and 11-azidoundec-1-ene. A. N. also edited and prepared figures for the manuscript. J. K. performed contact angle measurements. B. L. conducted XPS measurements, XPS fitting, sample pre-treatment, and contributed to fluorescence and Raman experiments. A. M. contributed to conceptualization and synthesized $\text{iPrNHC}^{\text{Alk}}$. J. L. synthesized Di-AlkNHC . V. S. contributed to conceptualization and performed electrochemical experiments as well as scanning electron measurements. T. M. S. contributed to conceptualization and performed XPS experiments as well as AFM scratch tests and NHC deposition. M. D. A. synthesized iPrNHC . P. J. R., C. M. C., and J. M. provided supervision, manuscript editing and reviewing, as well as data analysis and interpretation. The manuscript was written with contributions from all authors. All authors have reviewed and approved the final version of the manuscript.



Conflicts of interest

There are no conflicts to declare.

Data availability

The data supporting this article have been included as part of the SI. Supplementary information: details for the synthesis of NHCs, FTIR, ^1H -NMR and ^{13}C -NMR, photographs of the setup used for electrodeposition and fluorescence/Raman experiments, survey XPS, xyz coordinates of the DFT-optimized geometries, cyclic voltammograms for a functionalized Pt electrode, one-pot deposition, effect of activation of glassy carbon, full-range of the Raman EC-SHINERS e-deposition, and replicate for the contact angle measurements. See DOI: <https://doi.org/10.1039/d5sc03908h>.

Acknowledgements

This work is affiliated with the Carbon to Metal Coating Institute (C2MCI) at Queen's University and was funded by the Government of Canada's New Frontiers in Research Fund (NFRFT-2020-00573, grant recipient: Cathleen M. Crudden). This research was conducted as part of an undergraduate training program, made possible by funding from the C2MCI. We would like to acknowledge Emily Albright, Jyoti Kotecha, Megan Bruce from the C2MCI, as well as Isabelle Beaulieu from McGill University for their support and organization. We would also like to thank the NanoQAM platform (Université du Québec à Montréal) and Mathieu Rivard (McGill University) for access to Raman microscopes and fluorometer, and to Patricia Moraille (Université de Montréal) for assistance with AFM scratch tests. All DFT calculations were performed with support from the Digital Research Alliance of Canada, which granted access to cluster infrastructure.

Notes and references

- 1 H. W. Wanzlick and E. Schikora, Ein nucleophiles Carben, *Chem. Ber.*, 1961, **94**, 2389–2393.
- 2 K. Öfele, 1,3-Dimethyl-4-imidazolinyliden-(2)-pentacarbonylchrom ein neuer übergangsmetall-carbenkomplex, *J. Organomet. Chem.*, 1968, **12**, P42–P43.
- 3 E. Peris, Smart N-Heterocyclic Carbene Ligands in Catalysis, *Chem. Rev.*, 2018, **118**, 9988–10031.
- 4 M. Iglesias and L. A. Oro, A leap forward in iridium-NHC catalysis: new horizons and mechanistic insights, *Chem. Soc. Rev.*, 2018, **47**, 2772–2808.
- 5 M. N. Hopkinson, C. Richter, M. Schedler and F. Glorius, An overview of N-heterocyclic carbenes, *Nature*, 2014, **510**, 485–496.
- 6 G. Kaur, R. L. Thimes, J. P. Camden and D. M. Jenkins, Fundamentals and applications of N-heterocyclic carbene functionalized gold surfaces and nanoparticles, *Chem. Commun.*, 2022, **58**, 13188–13197.
- 7 S. Engel, E. C. Fritz and B. J. Ravoo, New trends in the functionalization of metallic gold: from organosulfur ligands to N-heterocyclic carbenes, *Chem. Soc. Rev.*, 2017, **46**, 2057–2075.
- 8 A. V. Zhukhovitskiy, M. J. MacLeod and J. A. Johnson, Carbene Ligands in Surface Chemistry: From Stabilization of Discrete Elemental Allotropes to Modification of Nanoscale and Bulk Substrates, *Chem. Rev.*, 2015, **115**, 11503–11532.
- 9 C. A. Smith, M. R. Narouz, P. A. Lummis, I. Singh, A. Nazemi, C. H. Li and C. M. Crudden, N-Heterocyclic Carbene in Materials Chemistry, *Chem. Rev.*, 2019, **119**, 4986–5056.
- 10 A. Inayeh, R. R. K. Groome, I. Singh, A. J. Veinot, F. C. de Lima, R. H. Miwa, C. M. Crudden and A. B. McLean, Self-assemble of N-heterocyclic carbenes on Au(111), *Nat. Commun.*, 2021, **12**, 4034.
- 11 C. M. Crudden, J. H. Horton, M. R. Narouz, Z. Li, C. A. Smith, K. Munro, C. J. Baddeley, C. R. Larrea, B. Drevniok, B. Thanabalasingam, A. B. McLean, O. V. Zenkina, Ebralidze, II, Z. She, H. B. Kraatz, N. J. Mosey, L. N. Saunders and A. Yagi, Simple direct formation of self-assembled N-heterocyclic carbene monolayers on gold and their application in biosensing, *Nat. Commun.*, 2016, **7**, 12654.
- 12 L. Jiang, B. Zhang, G. Medard, A. P. Seitsonen, F. Haag, F. Allegretti, J. Reichert, B. Kuster, J. V. Barth and A. C. Papageorgiou, N-Heterocyclic carbenes on close-packed coinage metal surfaces: bis-carbene metal adatom bonding scheme of monolayer films on Au, Ag and Cu, *Chem. Sci.*, 2017, **8**, 8301–8308.
- 13 Y. Choi, C. S. Park, H. V. Tran, C. H. Li, C. M. Crudden and T. R. Lee, Functionalized N-Heterocyclic Carbene Monolayers on Gold for Surface-Initiated Polymerizations, *ACS Appl. Mater. Interfaces*, 2022, **14**, 44969–44980.
- 14 C. R. Larrea, C. J. Baddeley, M. R. Narouz, N. J. Mosey, J. H. Horton and C. M. Crudden, N-Heterocyclic Carbene Self-assembled Monolayers on Copper and Gold: Dramatic Effect of Wingtip Groups on Binding, Orientation and Assembly, *ChemPhysChem*, 2017, **18**, 3536–3539.
- 15 J. F. DeJesus, M. J. Trujillo, J. P. Camden and D. M. Jenkins, N-Heterocyclic Carbenes as a Robust Platform for Surface-Enhanced Raman Spectroscopy, *J. Am. Chem. Soc.*, 2018, **140**, 1247–1250.
- 16 G. Wang, A. Ruhling, S. Amirjalayer, M. Knor, J. B. Ernst, C. Richter, H. J. Gao, A. Timmer, H. Y. Gao, N. L. Doltsinis, F. Glorius and H. Fuchs, Ballbot-type motion of N-heterocyclic carbenes on gold surfaces, *Nat. Chem.*, 2017, **9**, 152–156.
- 17 J. J. Navarro, M. Das, S. Tosoni, F. Landwehr, M. Heyde, G. Pacchioni, F. Glorius and B. Roldan Cuenya, Promoted Thermal Reduction of Copper Oxide Surfaces by N-Heterocyclic Carbenes, *J. Phys. Chem. C*, 2022, **126**, 17528–17535.
- 18 N. Kaeffer, D. Mance and C. Coperet, N-Heterocyclic Carbene Coordination to Surface Copper Sites in Selective Semihydrogenation Catalysts from Solid-State NMR Spectroscopy, *Angew. Chem. Int. Ed. Engl.*, 2020, **59**, 19999–20007.



19 N. Kaeffer, H. J. Liu, H. K. Lo, A. Fedorov and C. Coperet, An N-heterocyclic carbene ligand promotes highly selective alkyne semihydrogenation with copper nanoparticles supported on passivated silica, *Chem. Sci.*, 2018, **9**, 5366–5371.

20 I. M. Jensen, V. Clark, H. L. Kirby, N. Arroyo-Curran and D. M. Jenkins, Tuning N-heterocyclic carbene wingtips to form electrochemically stable adlayers on metals, *Mater. Adv.*, 2024, **5**, 7052–7060.

21 Y. Zeng, T. Zhang, M. R. Narouz, C. M. Crudden and P. H. McBreen, Generation and conversion of an N-heterocyclic carbene on Pt(111), *Chem. Commun.*, 2018, **54**, 12527–12530.

22 T. Zhang, S. B. Khomane, I. Singh, C. M. Crudden and P. H. McBreen, N-heterocyclic carbene adsorption states on Pt(111) and Ru(0001), *Phys. Chem. Chem. Phys.*, 2024, **26**, 4083–4090.

23 S. Dery, P. Bellotti, T. Ben-Tzvi, M. Freitag, T. Shahar, A. Cossaro, A. Verdini, L. Floreano, F. Glorius and E. Gross, Influence of N-Substituents on the Adsorption Geometry of OH-Functionalized Chiral N-Heterocyclic Carbene, *Langmuir*, 2021, **37**, 10029–10035.

24 E. Amit, R. Mondal, I. Berg, Z. Nairoukh and E. Gross, N-Heterocyclic Carbene Monolayers on Metal-Oxide Films: Correlations between Adsorption Mode and Surface Functionality, *Langmuir*, 2024, **40**, 10374–10383.

25 J. T. Lomax, E. Goodwin, M. D. Aloisio, A. J. Veinot, I. Singh, W.-T. Shiu, M. Bakiro, J. Bentley, J. F. DeJesus, P. G. Gordon, L. Liu, S. T. Barry, C. M. Crudden and P. J. Ragogna, Deposition of N-Heterocyclic Carbene on Reactive Metal Substrates—Applications in Area-Selective Atomic Layer Deposition, *Chem. Mater.*, 2024, **36**, 5500–5507.

26 J. Ren, M. Freitag, Y. Gao, P. Bellotti, M. Das, B. Schulze Lammers, H. Monig, Y. Zhang, C. G. Daniliuc, S. Du, H. Fuchs and F. Glorius, Reversible Self-Assembly of an N-Heterocyclic Carbene on Metal Surfaces, *Angew. Chem. Int. Ed. Engl.*, 2022, **61**, e202115104.

27 L. Stephens, J. D. Padmos, M. R. Narouz, A. Al-Rashed, C.-H. Li, N. Payne, M. Zamora, C. M. Crudden, J. Mauzeroll and J. H. Horton, The Structural and Electrochemical Effects of N-Heterocyclic Carbene Monolayers on Magnesium, *J. Electrochem. Soc.*, 2018, **165**, G139–G145.

28 L. Laundry-Mottiar, T. M. Suduwella, W. G. K. Senanayake, M. J. Turnbull, A. Juneau, E. Kaur, M. D. Aloisio, T. M. G. Selva, J. D. Henderson, H.-Y. Nie, M. Biesinger, J. J. Noel, Y. S. Hedberg, C. M. Crudden and J. Mauzeroll, N-Heterocyclic Carbene Overlays on Mild Steel, *Chem. Mater.*, 2024, **37**(1), 76–86.

29 I. Berg, E. Amit, L. Hale, F. D. Toste and E. Gross, N-Heterocyclic Carbene Based Nanolayer for Copper Film Oxidation Mitigation, *Angew. Chem. Int. Ed. Engl.*, 2022, **61**, e202201093.

30 A. J. Veinot, A. Al-Rashed, J. D. Padmos, I. Singh, D. S. Lee, M. R. Narouz, P. A. Lummis, C. J. Baddeley, C. M. Crudden and J. H. Horton, N-Heterocyclic Carbene Reduce and Functionalize Copper Oxide Surfaces in One Pot, *Chemistry*, 2020, **26**, 11431–11434.

31 J. S. G. Selva, Y. Li, J. Kaur, A. Juneau, A. Diraki, S. Bendahmane, J. D. Henderson, M. D. Aloisio, A. Messina, A. Nezamzadeh, C. J. Viasus Pérez, M. C. Biesinger, A. Levasseur, C. M. Crudden and J. Mauzeroll, N-Heterocyclic Carbene Deposition on a Copper Powder Surface Using Mechanochemistry, *ACS Appl. Mater. Interfaces*, 2025, **17**(6), 10004–10013.

32 D. T. H. Nguyen, S. Salek, L. R. Shultz-Johnson, M. Belanger-Bouliga, T. Jurca, J. C. Byers and A. Nazemi, Poly(N-Heterocyclic Carbene)-Capped Alloy and Core-Shell AuAg Bimetallic Nanoparticles, *Angew. Chem. Int. Ed. Engl.*, 2024, **63**, e202409800.

33 I. M. Jensen, S. Chowdhury, G. Hu, L. Jensen, J. P. Camden and D. M. Jenkins, Seeking a Au-C stretch on gold nanoparticles with (13)C-labeled N-heterocyclic carbene, *Chem. Commun.*, 2023, **59**, 14524–14527.

34 N. Bridonneau, L. Hippolyte, D. Mercier, D. Portehault, M. Desage-El Murr, P. Marcus, L. Fensterbank, C. Chaneac and F. Ribot, N-Heterocyclic carbene-stabilized gold nanoparticles with tunable sizes, *Dalton Trans.*, 2018, **47**, 6850–6859.

35 S. Wang, X. Yu, Y. Wang, B. Zhou, F. Shen and H. Cao, N-Heterocyclic carbene-functionalized metal nanoparticles and nanoclusters for nanocatalysis, *Dalton Trans.*, 2024, **53**, 18440–18450.

36 A. I. Sullivan, E. A. Steele, S. Takano, E. Zeinizade, J. Chen, S. Malola, K. Siddhant, H. Hakkinen, K. G. Stamplecoskie, T. Tsukuda, G. Zheng and C. M. Crudden, Diving into Unknown Waters: Water-Soluble Clickable Au(13) Nanoclusters Protected with N-Heterocyclic Carbene for Bio-Medical Applications, *J. Am. Chem. Soc.*, 2025, **147**(5), 4230–4238.

37 E. L. Albright, T. I. Levchenko, V. K. Kulkarni, A. I. Sullivan, J. F. DeJesus, S. Malola, S. Takano, M. Nambo, K. Stamplecoskie, H. Hakkinen, T. Tsukuda and C. M. Crudden, N-Heterocyclic Carbene-Stabilized Atomically Precise Metal Nanoclusters, *J. Am. Chem. Soc.*, 2024, **146**, 5759–5780.

38 R. M. Mayall, C. A. Smith, A. S. Hyla, D. S. Lee, C. M. Crudden and V. I. Birss, Ultrasensitive and Label-Free Detection of the Measles Virus Using an N-Heterocyclic Carbene-Based Electrochemical Biosensor, *ACS Sens.*, 2020, **5**, 2747–2752.

39 S. Kang, S. E. Byeon and H. J. Yoon, N-Heterocyclic Carbene Anchors in Electronics Applications, *Bull. Korean Chem. Soc.*, 2021, **42**, 712–723.

40 C. M. Crudden, J. H. Horton, I. I. Ebralidze, O. V. Zenkina, A. B. McLean, B. Drevniok, Z. She, H. B. Kraatz, N. J. Mosey, T. Seki, E. C. Keske, J. D. Leake, A. Rousina-Webb and G. Wu, Ultra stable self-assembled monolayers of N-heterocyclic carbene on gold, *Nat. Chem.*, 2014, **6**, 409–414.

41 D. T. Nguyen, M. Freitag, M. Korsgen, S. Lamping, A. Ruhling, A. H. Schafer, M. H. Siekman, H. F. Arlinghaus, W. G. van der Wiel, F. Glorius and B. J. Ravoo, Versatile Micropatterns of N-Heterocyclic Carbene on Gold Surfaces: Increased Thermal and Pattern





Stability with Enhanced Conductivity, *Angew. Chem. Int. Ed. Engl.*, 2018, **57**, 11465–11469.

42 J. Fan, S. Kang and M. Gupta, Long-term stability of N-heterocyclic carbene (NHC) functionalized organic electrochemical transistor (OECT) for biosensing applications, *Front. sens.*, 2024, **5**.

43 K. H. Kim, S. E. Seo, S. J. Park, J. Kim, C. S. Park, T. H. Le, C. S. Lee, Y. K. Kim, H. Y. Kim, S. Jun, J. Kwak, Y. K. Lee, H. Yoon, H. S. Song and O. S. Kwon, N-Heterocyclic Carbene–Graphene Nanotransistor Based on Covalent Bond for Ultrastable Biosensors, *Adv. Funct. Mater.*, 2024, **34**.

44 S. Park, S. Kang and H. J. Yoon, Thermopower of Molecular Junction in Harsh Thermal Environments, *Nano Lett.*, 2022, **22**, 3953–3960.

45 S. Qi, Q. Ma, X. He and Y. Tang, Self-assembled monolayers of N-heterocyclic carbene on gold: Stability under ultrasonic circumstance and computational study, *Colloids Surf. A*, 2018, **538**, 488–493.

46 E. Amit, L. Dery, S. Dery, S. Kim, A. Roy, Q. Hu, V. Gutkin, H. Eisenberg, T. Stein, D. Mandler, F. Dean Toste and E. Gross, Electrochemical deposition of N-heterocyclic carbene monolayers on metal surfaces, *Nat. Commun.*, 2020, **11**, 5714.

47 V. Smil, *Still the iron age: iron and steel in the modern world*, Butterworth-Heinemann, 2016.

48 M. C. Stackaruk, D. L. Stack, J. D. Masuda, R. D. Singer and C. L. Brosseau, Nanostructured Copper Screen-Printed Electrodes as a Platform for Plasmon-Enhanced Spectroelectrochemistry, *ACS Appl. Nano Mater.*, 2024, **7**, 8247–8257.

49 T. Yamamoto, M. Akahori, K. Natsui, T. Saitoh and Y. Einaga, Controlled decoration of boron-doped diamond electrodes by electrochemical click reaction (e-CLICK), *Carbon*, 2018, **130**, 350–354.

50 T. Heinrich, C. H. H. Traulsen, E. Darlatt, S. Richter, J. Poppenberg, N. L. Traulsen, I. Linder, A. Lippitz, P. M. Dietrich, B. Dib, W. E. S. Unger and C. A. Schalley, The versatility of “click” reactions: molecular recognition at interfaces, *RSC Adv.*, 2014, **4**, 17694–17702.

51 J. Kaur, G. Asadiankouhiehkhordi, V. Singh, A. C. Liberati, A. Diraki, S. Bendahmane, M. D. Aloisio, P. Patel, J. Henderson, F. Ben Ettouil, C. M. Crudden, M. Biesinger, A. Levasseur, C. Moreau and J. Mauzeroll, N-Heterocyclic carbene-promoted copper powder conditioning for thermal spray applications, *J. Mater. Chem. A*, 2025, **13**, 22745–22754.

52 L. Kuster, M. Belanger-Bouliga, T. E. Shaw, T. Jurca, A. Nazemi and M. Frenette, Insight into the nature of carbon–metal bonding for N-heterocyclic carbenes in gold/silver complexes and nanoparticles using DFT-correlated Raman spectroscopy: strong evidence for pi-backbonding, *Nanoscale*, 2024, **16**, 11052–11068.

53 T. Hartman, C. S. Wondergem and B. M. Weckhuysen, Practical Guidelines for Shell-Isolated Nanoparticle-Enhanced Raman Spectroscopy of Heterogeneous Catalysts, *ChemPhysChem*, 2018, **19**, 2461–2467.

54 J. F. Li, X. D. Tian, S. B. Li, J. R. Anema, Z. L. Yang, Y. Ding, Y. F. Wu, Y. M. Zeng, Q. Z. Chen, B. Ren, Z. L. Wang and Z. Q. Tian, Surface analysis using shell-isolated nanoparticle-enhanced Raman spectroscopy, *Nat. Protoc.*, 2013, **8**, 52–65.

55 M. H. Garcia, M. P. Robalo, A. R. Dias, M. T. Duarte, W. Wenseleers, G. Aerts, E. Goovaerts, M. P. Cifuentes, S. Hurst, M. G. Humphrey, M. Samoc and B. Luther-Davies, Synthesis and Nonlinear Optical Properties of η 5-Monocyclopentadienyliron(II) Acetylide Derivatives. X-ray Crystal Structures of $[\text{Fe}(\eta^5\text{-C}_5\text{H}_5)(\text{DPPE})(\text{p-C:CC}_6\text{H}_4\text{NO}_2)]$ and $[\text{Fe}(\eta^5\text{-C}_5\text{H}_5)(\text{DPPE})(\text{E-p-C:CC}_6\text{H}_4\text{C(H)C(H)C}_6\text{H}_4\text{NO}_2)]$, *Organometallics*, 2002, **21**, 2107–2118.

56 A. Mohammed, B. Minaev, H. Ågren, M. Lindgren and P. Norman, Classification of Raman active modes of platinum(II) acetylides: A combined experimental and theoretical study, *Chem. Phys. Lett.*, 2009, **481**, 209–213.

57 W. Li, Y. Li and K. Xu, Azidated Graphene: Direct Azidation from Monolayers, Click Chemistry, and Bulk Production from Graphite, *Nano Lett.*, 2020, **20**, 534–539.

58 J. J. Navarro, M. Das, S. Tosoni, F. Landwehr, J. P. Bruce, M. Heyde, G. Pacchioni, F. Glorius and B. Roldan Cuenya, Covalent Adsorption of N-Heterocyclic Carbenes on a Copper Oxide Surface, *J. Am. Chem. Soc.*, 2022, **144**, 16267–16271.

59 C. Gautier, I. López and T. Breton, A post-functionalization toolbox for diazonium (electro)-grafted surfaces: review of the coupling methods, *Mater. Adv.*, 2021, **2**, 2773–2810.

60 S. Smolka and K. Kruckiewicz, Catalyst Design through Grafting of Diazonium Salts–A Critical Review on Catalyst Stability, *Int. J. Mol. Sci.*, 2023, **24**.

61 M. Mooste, E. Kibena-Pöldsepp, M. Marandi, L. Matisen, V. Sammelselg, F. I. Podvorica and K. Tammeveski, Surface and electrochemical characterization of aryl films grafted on polycrystalline copper from the diazonium compounds using the rotating disk electrode method, *J. Electroanal. Chem.*, 2018, **817**, 89–100.

62 P. Fortgang, T. Tite, V. Barnier, N. Zehani, C. Maddi, F. Lagarde, A. S. Loir, N. Jaffrezic-Renault, C. Donnet, F. Garrelie and C. Chaix, Robust Electrografting on Self-Organized 3D Graphene Electrodes, *ACS Appl. Mater. Interfaces*, 2016, **8**, 1424–1433.

63 Y. R. Leroux, H. Fei, J. M. Noel, C. Roux and P. Hapiot, Efficient covalent modification of a carbon surface: use of a silyl protecting group to form an active monolayer, *J. Am. Chem. Soc.*, 2010, **132**, 14039–14041.

64 A. Mattiuzzi, Q. Lenne, J. Carvalho Padilha, L. Troian-Gautier, Y. R. Leroux, I. Jabin and C. Lagrost, Strategies for the Formation of Monolayers From Diazonium Salts: Unconventional Grafting Media, Unconventional Building Blocks, *Front. Chem.*, 2020, **8**, 559.

65 M. Wróbel, D. M. Cegielka, A. Asyuda, K. Koziel, M. Zharnikov and P. Cyganik, N-heterocyclic carbenes – The design concept for densely packed and thermally ultra-stable aromatic self-assembled monolayers, *Nano Today*, 2023, **53**.

66 D. Hetemi, V. Noel and J. Pinson, Grafting of Diazonium Salts on Surfaces: Application to Biosensors, *Biosensors*, 2020, **10**.

67 A. Afzal, H. M. Siddiqi, S. Saeed and Z. Ahmad, Exploring resin viscosity effects in solventless processing of nano-SiO₂/epoxy polymer hybrids, *RSC Adv.*, 2013, **3**.

68 S. D. Place and P. Kavanagh, Electrochemical alcohol oxidation using a TEMPO nitroxide polymer as a homogeneous and surface-confined catalyst, *Electroanalysis*, 2024, **36**.

69 M. Rafiee, K. C. Miles and S. S. Stahl, Electrocatalytic Alcohol Oxidation with TEMPO and Bicyclic Nitroxyl Derivatives: Driving Force Trumps Steric Effects, *J. Am. Chem. Soc.*, 2015, **137**, 14751–14757.

70 C. M. Schroeder, F. Politano, K. K. Ohlhorst and N. E. Leadbeater, Acetamido-TEMPO mediated electrochemical oxidation of alcohols to aldehydes and ketones, *RSC Adv.*, 2023, **13**, 25459–25463.

71 F. Geneste, C. Moinet, S. Ababou-Girard and F. Solal, Covalent attachment of TEMPO onto a graphite felt electrode and application in electrocatalysis, *New J. Chem.*, 2005, **29**.

72 O. Swiech, R. Bilewicz and E. Megiel, TEMPO coated Au nanoparticles: synthesis and tethering to gold surfaces, *RSC Adv.*, 2013, **3**.

73 M. Seif-Eddine, S. J. Cobb, Y. Dang, K. Abdiaziz, M. A. Bajada, E. Reisner and M. M. Roessler, Operando film-electrochemical EPR spectroscopy tracks radical intermediates in surface-immobilized catalysts, *Nat. Chem.*, 2024, **16**, 1015–1023.

74 N. Mohebbati, A. Prudlik, A. Scherkus, A. Gudkova and R. Francke, TEMPO-Modified Polymethacrylates as Mediators in Electrosynthesis – Redox Behavior and Electrocatalytic Activity toward Alcohol Substrates, *ChemElectroChem*, 2021, **8**, 3837–3843.

75 M. A. Pellitero, I. M. Jensen, N. L. Dominique, L. C. Ekowo, J. P. Camden, D. M. Jenkins and N. Arroyo-Curra, Stability of N-Heterocyclic Carbene Monolayers under Continuous Voltammetric Interrogation, *ACS Appl. Mater. Interfaces*, 2023, **15**, 35701–35709.

76 T. Bystron, E. Sramkova, F. Dvorak and K. Bouzek, Glassy carbon electrode activation – A way towards highly active, reproducible and stable electrode surface, *Electrochim. Acta*, 2019, **299**, 963–970.

77 A. M. Abdel-Aziz, H. H. Hassan and I. H. A. Badr, Activated Glassy Carbon Electrode as an Electrochemical Sensing Platform for the Determination of 4-Nitrophenol and Dopamine in Real Samples, *ACS Omega*, 2022, **7**, 34127–34135.

78 J. Zhang, D. Ma, D. Du, Z. Xi and L. Yi, An efficient reagent for covalent introduction of alkynes into proteins, *Org. Biomol. Chem.*, 2014, **12**, 9528–9531.

79 J. Sinha, R. Sahoo and A. Kumar, Processable, Regioregular, and “Click”able Monomer and Polymers Based on 3,4-Propylenedioxythiophene with Tunable Solubility, *Macromolecules*, 2009, **42**, 2015–2022.

80 W. Haiss, N. T. Thanh, J. Aveyard and D. G. Fernig, Determination of size and concentration of gold nanoparticles from UV-vis spectra, *Anal. Chem.*, 2007, **79**, 4215–4221.

81 N. Fairley, V. Fernandez, M. Richard-Plouet, C. Guillot-Deudon, J. Walton, E. Smith, D. Flahaut, M. Greiner, M. Biesinger, S. Tougaard, D. Morgan and J. Baltrusaitis, Systematic and collaborative approach to problem solving using X-ray photoelectron spectroscopy, *Appl. Surf. Sci. Adv.*, 2021, **5**.

82 D. J. Morgan, The Utility of Adventitious Carbon for Charge Correction: A Perspective From a Second Multiuser Facility, *Surf. Interface Anal.*, 2024, **57**, 28–35.

83 M. J. Frisch, G. W. Trucks, H. B. Schlegel, G. E. Scuseria, M. A. Robb, J. R. Cheeseman, G. Scalmani, V. Barone, G. A. Petersson, H. Nakatsuji, *et al.*, *Gaussian 16 Rev. C.01*, 2016.

84 S. Tardio and P. J. Cumpson, Practical estimation of XPS binding energies using widely available quantum chemistry software, *Surf. Interface Anal.*, 2017, **50**, 5–12.

85 C. Lee, W. Yang and R. G. Parr, Development of the Colle-Salvetti correlation-energy formula into a functional of the electron density, *Phys. Rev. B: Condens. Matter Mater. Phys.*, 1988, **37**, 785–789.

86 A. D. Becke, Density-functional thermochemistry. III. The role of exact exchange, *J. Chem. Phys.*, 1993, **98**, 5648–5652.

87 S. H. Vosko, L. Wilk and M. Nusair, Accurate spin-dependent electron liquid correlation energies for local spin density calculations: a critical analysis, *Can. J. Phys.*, 1980, **58**, 1200–1211.

88 P. J. Stephens, F. J. Devlin, C. F. Chabalowski and M. J. Frisch, Ab Initio Calculation of Vibrational Absorption and Circular Dichroism Spectra Using Density Functional Force Fields, *J. Phys. Chem.*, 2002, **98**, 11623–11627.

89 A. V. Marenich, C. J. Cramer and D. G. Truhlar, Universal solvation model based on solute electron density and on a continuum model of the solvent defined by the bulk dielectric constant and atomic surface tensions, *J. Phys. Chem. B*, 2009, **113**, 6378–6396.

